Photoinduced Tip–Sample Forces for Chemical Nanoimaging and Spectroscopy

Brian T. O'Callahan,[ID] Jun Yan, Fabian Menges, Eric A. Muller,[ID] and Markus B. Raschke*[ID]

Department of Physics, Department of Chemistry, and JILA, University of Colorado at Boulder, Boulder, Colorado 80309, United States

S *Supporting Information*

ABSTRACT: Control of photoinduced forces allows nanoparticle manipulation, atom trapping, and fundamental studies of light-matter interactions. Scanning probe microscopy enables the local detection of photoinduced effects with nano-optical imaging and spectroscopy modalities being used for chemical analysis and the study of physical effects. Recently, the development of a novel scanning probe technique has been reported with local chemical sensitivity attributed to the localization and detection of the optical gradient force between a probe tip and sample surface via infrared vibrationally resonant coupling. However, the magnitude and spectral line shape of the observed signals disagree with theoretical predictions of optical gradient forces.

Here, we clarify this controversy by resolving and analyzing the interplay of several photoinduced effects between scanning probe tips and infrared resonant materials through spectral and spatial force measurements. Force spectra obtained on IR-active vibrational modes of polymer thin films are symmetric and match the material absorption spectra in contrast to the dispersive spectral line shape expected for the optical gradient force response. Sample thickness dependence shows continuous increase in force signal beyond the thickness where the optical dipole force would saturate. Our results illustrate that photoinduced force interactions between scanning probe tips and infrared-resonant materials are dominated by short-range thermal expansion and possibly long-range thermally induced photoacoustic effects. At the same time, we provide a guideline to detect and discriminate optical gradient forces from other photoinduced effects, which opens a new perspective for the development of new scanning probe modalities exploiting ultrastrong opto-mechanical coupling effects in tip–sample cavities.

KEYWORDS: *Chemical nanoimaging, optical force, photothermal, infrared spectroscopy, PiFM, PTIR*
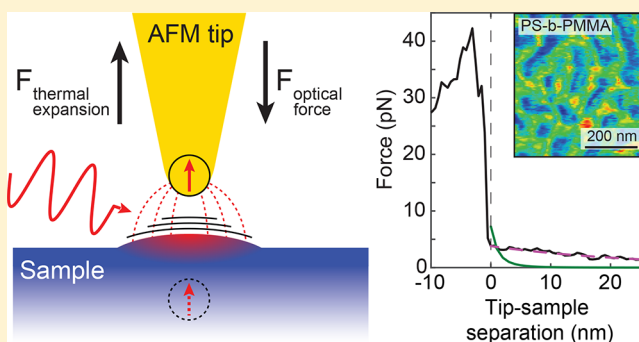
Optical forces are used as optical tweezers for nanoparticle manipulation,[1] for atom trapping,[2] and in cavity-optomechanics[3] and are the focus of much recent research into fundamental physical phenomena including the Casimir–Polder force.[4] A proposed method for measuring optical forces uses the tip of an atomic force microscope (AFM) at nanometer proximity to a sample. In this implementation, light illumination of the tip creates an electric polarization density p at the tip apex, which induces a coupled polarization density p' in the sample. The resulting mutual electromagnetic force is given by $\vec{F} = \vec{p} \cdot \nabla \vec{E}$ with the optical field $\vec{E}$. This so-called optical gradient force has been proposed as the contrast mechanism for several recent AFM-based studies which have demonstrated chemical specificity with nanoscale spatial resolution, indicating a powerful new imaging and nanospectroscopy modality complementing scattering-scanning near-field optical microscopy (s-SNOM)[5−10] and photothermal infrared microscopy.[11−13]

However, these studies have painted a confusing picture regarding the actual contrast mechanism. Whereas some studies assign the contrast to the optical gradient force,[5−10] others assign it to material absorption and thermal expansion.[11−13] The observed force magnitudes vary from 0.85−2.7 pN with force gradients ranging from 2.1−3.7 × 10⁻⁵ N/m.[9,10] However, theory predicts optical gradient force magnitudes over 2 orders of magnitude weaker under the typical experimental conditions at IR frequencies.[14−16] Further, measured spectra of the photoinduced force exhibit an absorptive line shape,[8,17] whereas theory predicts a dispersive spectral line shape for the optical gradient force.[14,18]

In addition to an optical gradient force, several competing forces associated with photoexcitation exist and require careful consideration. For example, absorption and subsequent heating of the sample material results in thermal expansion, which underlies, e.g., photoacoustic imaging and tomography.[19] Additionally, an AFM tip can detect thermal expansion and opto-mechanical forces providing for chemical nanoimaging contrast with down to monolayer sensitivity.[11−13]
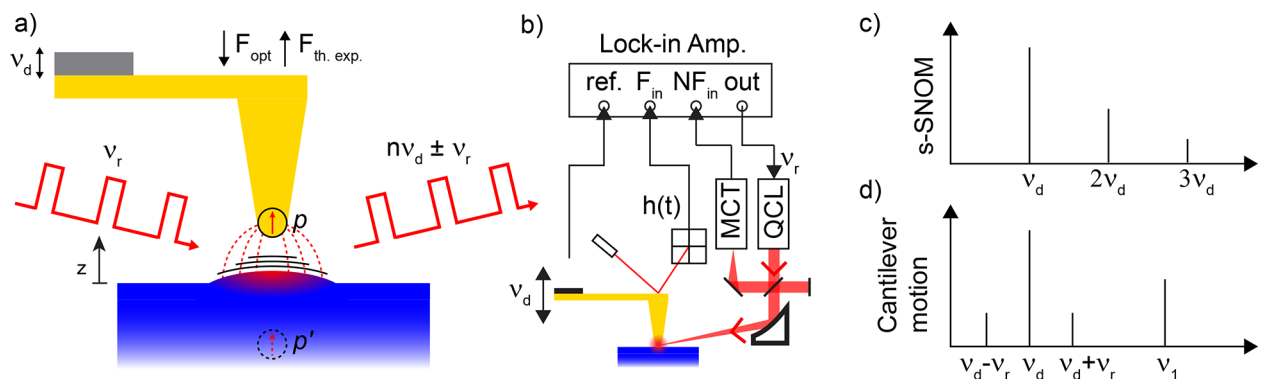
Figure 1. (a) Photoinduced force experiment: mid-infrared light pulsed at repetition rate ν_r illuminates the tip–sample gap with possible optical dipole force $F_{opt.}$ and thermal expansion-induced impulsive force $F_{th.exp.}$ indicated and simultaneous s-SNOM mode collecting tip-scattered near-field. (b) Lock-in amplifier receives tip dither frequency ν_d, tip motion $h(t)$, and s-SNOM near-field signal NF_{in} demodulating at harmonics of the tip motion $n\nu_d$. Fourier components of (c) s-SNOM signal and (d) cantilever dynamics with sidebands at frequencies $\nu_d \pm \nu_r$ due to mixing of cantilever motion and the photoinduced forces.
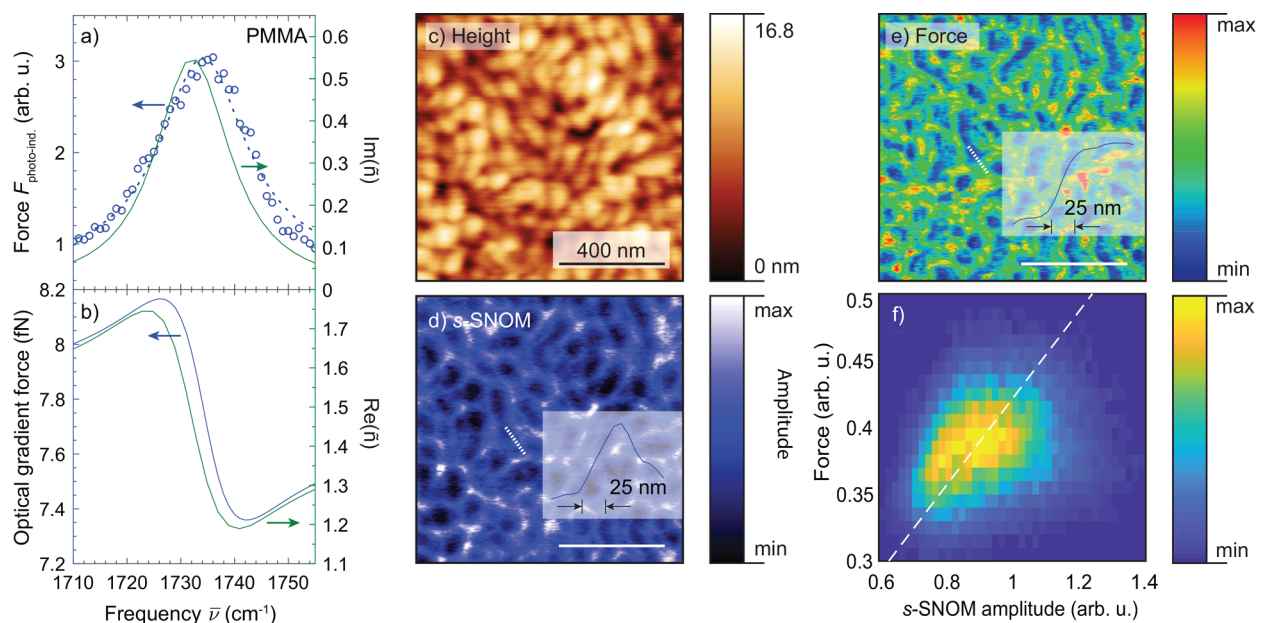

Figure 2. (a) Measured force spectrum of carbonyl resonance of PMMA (blue) with corresponding Lorentzian fit (dashed) matches the imaginary part of the index of refraction $Im(\tilde{n}) = \kappa$ (green).[22] (b) Theoretical optical gradient force spectrum calculated using eq 1 and the real part of index of refraction $Re(\tilde{n})$ both show dispersive behavior. (c) AFM topography, (d) s-SNOM amplitude, (e) and force signal of a PS−PMMA block copolymer sample with laser tuned to the carbonyl resonance at $\bar{\nu}_{C=O} = 1735\ cm^{-1}$. The force signal shows high contrast with strong signal on PMMA with ∼25 nm spatial resolution and correlated with the s-SNOM amplitude (f).

To resolve this controversy and distinguish different competing photoinduced forces between a tip and sample, we perform correlated and quantitative nanoscale spatial and IR spectral local-probe measurements. We observe symmetric force spectra that match the sample absorption spectrum, and measure force magnitudes up to 40 pN. Sample thickness dependent measurements reveal a signal increase scaling over hundreds of nanometers in film thickness, whereas the optical gradient force is expected to saturate at distances of tens of nanometers, scaling with the tip apex radius. Further, tip–sample distance-dependent measurements indicate that the dominant force is related to direct physical tip–sample contact. We observe comparably weak spatially extended forces out to few tens of nanometers distances from the sample surface that can be attributed to photothermally induced acoustic interactions. The combined results thus strongly support that thermal expansion is the dominant contrast mechanism and

can explain the vast majority of photoinduced force-based chemical imaging results to date.

Experiment. Figure 1a shows the experimental approach based on an AFM (modified Vesta AFM-SP, Anasys Instruments) operating in dynamic mode feedback by driving and monitoring the cantilever motion at its fundamental resonant frequency $\nu_d = \nu_0$. A lock-in amplifier (HF2LI, Zurich Instruments) receives the tip drive signal and the tip motion $(h(t))$, as measured by a laser diode reflected off the backside of the cantilever onto a four-quadrant photodiode (Figure 1b). A TTL pulse output triggers a pulsed mid-IR quantum cascade laser (QCL, Daylight solutions) at a frequency ν_r set by an internal oscillator in the lock-in amplifier. A high numerical aperture (NA = 0.48) off-axis parabolic mirror focuses the IR radiation onto the apex of the tip. In addition to the photoinduced forces $F_{photo−ind}$, the near-field s-SNOM response can also be monitored by collecting tip-scattered light, measured

with a mercury−cadmium−telluride (MCT) detector and demodulating at higher harmonics of the tip motion $n\nu_d$ for integers n (Figure 1c).[20]

The photoinduced force signal relies on the presence of a force gradient due to a nonuniform photoinduced force, which results in a varying force magnitude during a tip oscillation cycle as described previously.[5−8] The force gradient and the periodic excitation of the tip−sample forces at the laser repetition rate ν_r gives rise to a corresponding tip motion at sideband frequencies $\nu_0 \pm \nu_r$ due to the nonlinear mixing between the tip motion and the time varying photoinduced force (Figure 1d).[21] We set ν_r to the difference of the first two vibrational frequencies of the cantilever ν_0 and ν_1, that is, $\nu_r = \nu_1 - \nu_0$. The photoinduced forces then resonantly drive the second bending mode, which dramatically improves sensitivity.

In an alternative technique, the second bending mode is used for AFM feedback ($\nu_d = \nu_1$), and the first bending mode is used to monitor the photoinduced force. This variation permits operation using smaller tapping amplitudes due to the higher effective spring constant of the second bending mode, and improves sensitivity to strongly surface-confined forces.

We obtain spectra of the photoinduced force by sweeping the laser wavelength. As model systems, we investigate the carbonyl (C=O) resonance of PMMA at $\bar{\nu} = 1735$ cm^{-1} and the symmetric C−F stretches in polytetrafluoroethylene (PTFE) at $\bar{\nu} \approx 1152$ cm^{-1}. Block copolymer samples were prepared by spin-coating a 1% w/v solution of PS-*b*-PMMA in toluene onto a native oxide silicon substrate. For the sample thickness-dependent measurements, a 1% w/v solution of PMMA in toluene was spin-coated on a silicon substrate tilted at an ∼15° angle to create a tapered PMMA film with variable film thickness. The humidity during measurements is controlled by flowing dry air into the AFM enclosure.

Results. Figure 2a shows the measured force spectrum of the PMMA sample normalized against a Si reference sample (circles) with a corresponding Lorentzian fit (dashed). The force is peaked at the carbonyl resonance of PMMA, and the symmetric spectral line shape matches that of the imaginary part of the dielectric function $\text{Im}(\tilde{n}) = \kappa(\omega)$ obtained from ellipsometry[22] (green) within ±1.5 cm^{-1} accuracy.

We calculate the expected optical gradient force using the dipole approximation to represent the polarizabilities of the tip and sample to first order. In the dipole approximation, the sample is treated as a semi-infinite half-space and the tip as a sphere of radius r with polarizability $\alpha_t = 4\pi r^3 \epsilon_0 \frac{\epsilon_t - 1}{\epsilon_t + 2}$ with ϵ_t the dielectric function of the tip (see Supporting Information for additional model details). When the tip is close to the sample surface, the mutual interaction and coupling between tip and sample gives rise to a modified tip polarization of $p = \alpha_t \left(E_0 + \frac{\beta p}{16\pi \epsilon_0 (r+h)^3} \right)$, where the second term is the radiation reaction term, $\beta = \frac{\epsilon_s(\omega) - 1}{\epsilon_s(\omega) + 1}$, and $\epsilon_s(\omega)$ is the dielectric function of the sample. Solving the recursive relation for p yields an effective polarizability $\alpha_{\text{eff}} = p/E_0 = \frac{\alpha_t}{(1 - \beta \alpha_t / 16\pi \epsilon_0 (r+h)^3)}$ that describes the combined tip−sample system.[20] The field acting on the tip dipole $E = E_0 + \frac{\beta \alpha_{\text{eff}} E_0}{16\pi \epsilon_0 (r+h)^3}$ thus gives rise to an attractive force toward the sample given by

$$\vec{F}_{\text{opt.}} = \vec{p} \cdot \nabla \vec{E} = \text{Re}\left(\alpha_{\text{eff}}^2 \frac{3E_0^2}{16\pi \epsilon_0 (r+h)^4} \right) \quad (1)$$

We used a sphere radius of $r = 10$ nm to represent the tip apex radius of our commercially acquired tips (240AC-GG OPUS, Mikromasch, spring constant $k \approx 2$ N/m). As shown in Figure 2b, the calculated force using eq 1 is in the sub-10 fN range, and shows a dispersive line shape, which is in agreement with recent electromagnetic simulations[14] and analytic theory.[17,23] Its line shape resembles the real part of the index of refraction (green). Although this model for the coupled tip−sample polarizability does not consider the extended geometry of the tip shaft or nanoscale surface corrugations at the tip apex, it correctly describes the key physical principle and has been successfully applied to previous near-field spectroscopic studies.[24,25]

By raster-scanning the tip across the sample surface, using the first cantilever mode for AFM feedback, we then obtain spatial images with resolution given by the tip apex radius of ∼25 nm. Figure 2c shows the topography image of the PS-*b*-PMMA sample. The carbonyl resonant *s*-SNOM image at $\bar{\nu} = 1735$ cm^{-1} shows strong signal on the PMMA domains (Figure 2d) correlated with the force signal (Figure 2e), both with ∼25 nm spatial resolution (inset), with correlation plot shown in Figure 2f.

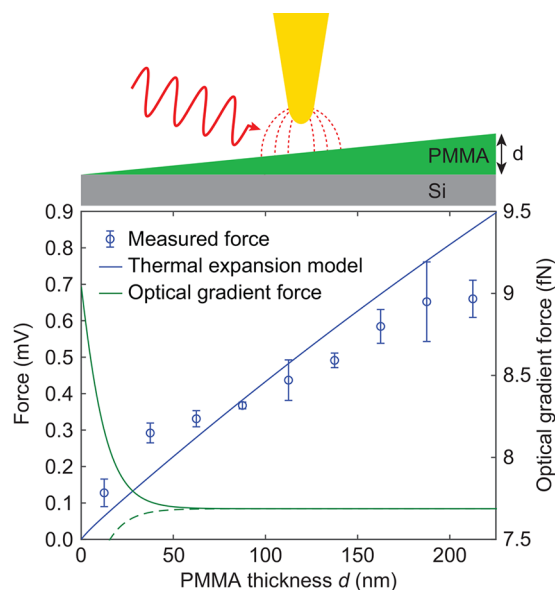Figure 3 shows the PMMA film thickness dependence of the photoinduced force signal at the carbonyl resonance frequency

Figure 3. Photoinduced force dependence on PMMA thickness (blue symbols). The relative thermal expansion calculated from eq 3 (blue line), and optical gradient force calculated for the PMMA/Si layered system (green, solid) and for a free-standing PMMA layer (green, dashed) are shown for comparison.

measured on the tapered PMMA film with thickness ranging from ≃7−250 nm (blue). The measured force monotonically increases over the entire thickness range. We calculate the film thickness dependent thermal expansion based on the electric field intensity within the PMMA film given by

$$E(z) = \frac{\alpha_{\text{eff}} E_0}{2\pi \epsilon_0 \epsilon_2(\omega)(z+h)^3} + E_0 e^{-z/2\delta} \quad (2)$$
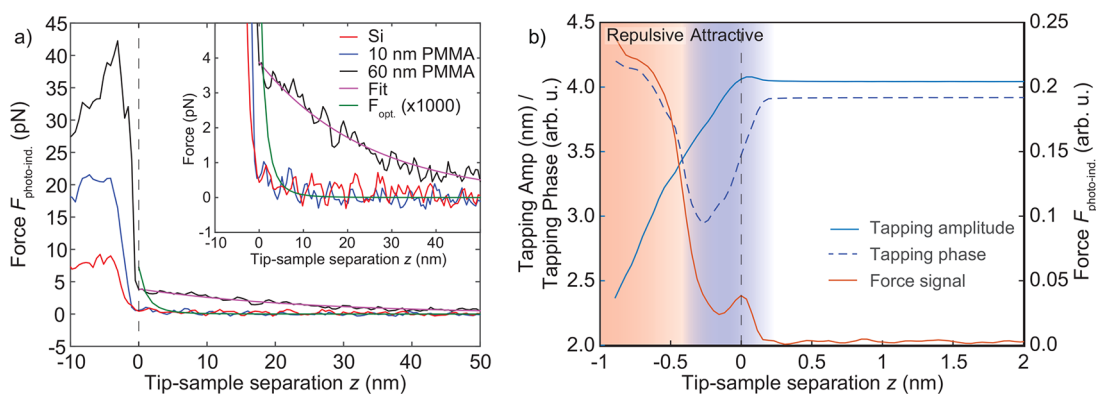
Figure 4. a) Photoinduced force approach curves on a 60 nm thick PMMA film (black), 10 nm thick PMMA film (blue), and Si (red) at the carbonyl resonance ($\bar{\nu} = 1735$ cm^{-1}). For each sample, a prominent increase in signal occurs only at the point of tip−sample contact ($z = 0$ nm). Only for the 60 nm film, a long-range force described by an exponential decay (magenta) with decay length $l = 25$ nm is observed. Predictions from the point-dipole model for the optical gradient force are shown in green. (b) Approach curve measurement over a PTFE surface, with laser tuned to resonance with the C—F symmetric stretch at $\bar{\nu} = 1152$ cm^{-1}. A weak attractive force is observed before the onset of the repulsive thermal expansion.

Table 1. Key Characteristics of Photo-Induced Forces along with the Predicted Characteristics of the Force Due to Direct Thermal Expansion, the Optical Gradient Force, and the Photoacoustic Force[a]

[a]The experimentally observed features match a combination of direct thermal expansion and minor photo-acoustic force contributions and disagree with all characteristics of the optical gradient force in spectral, distance, and thickness dependence.

with the intensity absorption depth of PMMA $\delta \approx 0.8$ μm determined by Beer's law, the complex dielectric function of PMMA $\epsilon_2(\omega)$, and distance z from the PMMA/air interface. The first term describes the localized evanescent electric field between the tip and sample based on the dipole approximation from above. The second term is the exponential decay of far-field illumination within the PMMA layer. The thermal expansion Δz is then obtained for a given film thickness t using

$$\Delta z(t) \propto \alpha_{T,PMMA} \int_0^t |E(z)|^2 dz + \alpha_{T,Si} \int_t^\infty |E(z)|^2 dz$$

(3)

where $\alpha_{T,x}$ is the thermal expansion coefficient with $x =$ Si, PMMA. The calculated thermal expansion (blue line) shows an increase with t up to the absorption depth of PMMA $\delta = 0.8$ μm. In contrast, the optical gradient force (green) is largely

thickness-independent with only a slight increase below a film thickness of 30 nm for the PMMA/Si sample structure due to the higher IR dielectric function of Si.

Figure 4a shows approach curves on the PMMA films of 60 nm (black), and 10 nm (blue) thicknesses, and the bare Si surface with laser tuned to the carbonyl resonance at $\bar{\nu}$ = 1735 cm^{-1}. In each case the force signal rises sharply at tip−sample contact (z = 0 nm). Only for the 60 nm case, an order of magnitude weaker long-range component emerges. This spatially extended force fits well to an exponential decay with $1/e$ decay length l = 25 nm (magenta). This force is correlated with a slight decrease in the tapping phase, indicating a repulsive character (see Supporting Information). Fits to a power law $F(z)$ ∝ z^{α} for $\alpha > 0$, generally give worse agreement to the measured distance dependence. The calculated distance dependence of the optical gradient force (green) shown for comparison is confined to tip−sample separations on the order of the tip apex radius $r \simeq 20$ nm. Note that a spectrum acquired 15 nm from tip−sample contact above the 60 nm thick PMMA film shows a symmetric line shape, closely matching the absorption profile of PMMA (see Supporting Information). These results indicate that the long-range force is associated with optical absorption.

We additionally performed approach curves using small, for example, as low as 2 nm tapping amplitudes to improve sensitivity to the possible optical gradient force acting on short length scales. However, only a similarly sharp rise in force at direct tip−sample contact is observed, even at the lowest tapping amplitudes of 2 nm, with no discernible long-range behavior (see Supporting Information).

Finally, we investigate weak tip−sample interactions occurring within the first few nanometers of the surface that could be obscured by damping from adsorbed surface water. In order to reduce effects of the adsorbed water layer, we examine the hydrophobic surface of PTFE under a dry-air-purged environment as described above (relative humidity RH < 2%). We tune the laser to $\bar{\nu}$ = 1152 cm^{-1}, which is resonant with the C—F symmetric stretch vibration[26] and use small tapping amplitudes in the range 4−10 nm in order to increase sensitivity to few nanometers short-range forces. As shown in Figure 4b, we measure the tapping amplitude, tapping phase, and force signal as a function of tip−sample distance. When the tip is within <1 nm of the sample, the tapping amplitude increases slightly and the tapping phase dips, as expected for attractive van der Waals interactions between tip and sample.[27−29] With further approach toward the sample, the tapping amplitude decreases and the tapping phase increases as the tip reaches the repulsive interaction regime. The simultaneously measured force signal is zero away from the sample, increasing slightly during the attractive region of tip−sample interactions, and then increasing further by an order of magnitude through the repulsive tip−sample interaction region. From these measurements of tip−sample forces in the absence of adsorbed water, we have increased sensitivity to the small optically induced forces between tip and sample that occur within <1 nm, however the dominant interaction still occurs within the repulsive interaction regime and can be assigned to thermal expansion forces.

Discussion. In the following, we will discuss our results in relation to previous reports of photoinduced tip−sample interaction forces and with respect to some key characteristics of the different photoinduced forces displayed in Table 1.

In agreement with previous results,[8] we observe a spectral dependence of the photoinduced force that is symmetric and matches the IR absorption spectrum. This is in contrast to the

predicted dispersive line shape for the optical gradient force as shown in Figure 2b. Note that in ref 8 a symmetric line shape was previously assigned to the experimental observation of the optical gradient force by a technique subsequently termed photoinduced force microscopy (PiFM). This conclusion has been drawn based in part on neglecting the radiation reaction term as described above, resulting in the reduced expression $F \propto \mathrm{Re}(\alpha_t \alpha_s^*) = \alpha_t' \alpha_s' + \alpha_t'' \alpha_s''$ for tip and sample polarizabilities $\alpha_{t,s}$ respectively, which was assumed to be dominated by $\alpha_t'' \alpha_s''$. However, for metallic tips as used in these and our experiments $\epsilon_t' \gg \epsilon_t''$ at infrared frequencies and thus the product of the real parts of the polarizability dominates.

A second criteria relevant to identify the physical origin of the photoinduced signal is the force magnitude. For a 10 nm thick PMMA layer on-resonance we estimate a force magnitude of 20 pN. Using the cantilever spring constant of $k \sim 2$ N/m and Hooke's law for the thermal expansion force $F_{\mathrm{th.exp.}} = k\delta h$, this corresponds to a displacement of $\delta h \approx 8$ pm, or a local heating of the PMMA surface of $\Delta T \approx 16$ K, which agrees with our estimate of sample heating due to IR absorption. The force magnitude estimate is based on assigning the observed noise floor of the force signal as the minimum detectable force ΔF_{rms} limited by thermal noise which is expressed by $\Delta F_{\mathrm{rms}} = \sqrt{(4k_B T/Q\omega k)}$ where T is temperature, k_B is Boltzmann's constant, and k and Q are the cantilever spring constant and the quality factor of the cantilever vibrational mode, respectively. For our cantilevers operated at room temperature $F_{\mathrm{rms}} \approx 0.3$ pN, which is much larger than the optical gradient force magnitude predicted based on a spherical dipole model[14] (~8 fN for the force between a gold and a PMMA sphere), and underscores the difficulty of detecting the optical gradient force under conventional AFM operation, especially when competing photoinduced forces are present. We note that the spherical dipole model used for these predictions does not capture the more extended geometry of the tip and the sample surface and can thereby potentially underestimate the magnitude of the optical gradient force by up to an order of magnitude. Models which incorporate a more extended tip structure may result in higher force values, yet predict similar dispersive lineshapes when applied.[30] Nevertheless, recent PiFM studies reporting peak force magnitudes in the tens of pN range[5,9,10] observed under similar experimental conditions as those reported here might not be related to the observation of optical gradient forces and can at least be equally well explained by local heating and thermal expansion effects.

Another approach to discriminate the various contributing forces is based on their dependence on sample thickness. While our measured force dependence on the PMMA film thickness matches calculations of thermal expansion dependence on thickness given in eq 3, it is in stark contrast to those calculated for the optical gradient force, which shows a qualitatively different trend. While the calculated optical gradient force has a maximum value at zero PMMA thickness and decays within about 30 nm, the force due to thermal expansion increases with film thickness up to approximately the absorption depth of $\delta \approx$ 0.8 μm and is roughly linear for thickness <300 nm. This trend is corroborated by a recent time-resolved measurement of the photoinduced force indicating that thermo-mechanical effects dominate tip−sample interactions under impulsive laser excitation.[31] In contrast to the thermal expansion force, the optical gradient force is peaked at zero thickness due to the larger force magnitude between the tip and the Si substrate since

Si has a larger IR polarizability than PMMA. The thickness dependence of the optical gradient force is expected to scale qualitatively similar to the s-SNOM probe depth because the thickness dependence is incorporated through α_{eff}, which has the same form for the optical gradient force and the near-field scattering cross-section in s-SNOM. For comparison, we also plotted the corresponding thickness dependence of a free-standing PMMA film (green dashed line in Figure 3) showing a similar saturation within thickness values of ~30 nm.

Beyond the key characteristics discussed so far, recent studies have ascribed the observation of long-range interactions observed during approach curve measurements to an optical gradient force acting directly on the tip.[8,32] Although these studies provide incomplete evidence for the observation of optical gradient forces based on the criteria discussed above, we note that capillary forces due to the surface water layer and van der Waals forces could contribute to observed attractive forces acting at few nm distances from the sample surface such as those observed in Figure 4b. In particular, thermal expansion has recently been suggested to decrease the tip-sample separation and thus yield an attractive interaction because of the earlier onset of the van der Waals force. This effect has been proposed as an explanation for the discrepancy between the observed and predicted spectra of the optical gradient force.[17] Note that this effect would exhibit the same spectral and sample thickness dependencies as $F_{th.\ exp}$, though would show a distinct distance dependence. Calculations showing that small displacements of a surface can result in significant changes in the van der Waals forces between nearby objects resulting in heat transfer across a vacuum gap are presented in refs 33 and 34. Our results provide direct evidence that there are two or more long-range forces possible, because we separately observe an attractive force (Figure 4b) and a repulsive force with an absorptive spectral profile (Figure 4a), depending on sample material.

The observed long-range repulsive force might be caused by an impulsive thermal expansion of the sample that creates acoustic air waves, which in turn exert a force on the cantilever. During thermal expansion, the sample expands at the speed of sound of the material, much faster than the speed of sound in air, and thus can create propagating acoustic shock waves associated with a sudden, stepwise change in the spatial profile of air pressure.[35,36] At ambient pressure, and assuming a thermal expansion distance of 1−10 pm, the energy in the acoustic waves is on the order of a few femtojoules, which is comparable to the oscillation energy of the cantilever at tens of nanometers tapping amplitude. Thus, this could induce a cantilever motion at tip−sample separations below the mean free path of air molecules (~70 nm). The stepwise change in air pressure exerting an impulsive force on the cantilever is confined to the near-surface region due to the associated high wave-vectors of the wavefront, similar to evanescent electromagnetic waves. This could explain the good agreement of the force distance dependence to an exponential decay, instead of a steeper power law dependence predicted for the optical gradient force. While the observation of a long-range force signal alone does not provide definitive evidence for an optical gradient force, the characteristics of spectral line shape, magnitude, distance dependence, and sample thickness dependence at resonant IR frequencies strongly suggest that the dominant photoinduced forces directly relate to thermal expansion and secondary photoacoustic effects.

Finally, we note that in studies at optical frequencies the force spectra can show dispersive profiles[5,17] and show indications in spatial images of an optical gradient contribution to the signal.[6,7]

As noted previously,[14] the optical gradient forces at optical frequencies can be much stronger than their counterparts in the infrared, especially for electronically resonant materials with higher dielectric values and larger transition dipoles compared to local vibrational oscillators. However, optical absorption and thermal expansion can also provide significant contrast at visible frequencies, as demonstrated by ref 37.

In summary, we demonstrated that various competing photoinduced forces acting between scanning probe tips and IR resonant materials can contribute to the imaging contrast in scanning-probe-based force measurements under photoexcitation. Our results show that, depending on the sample thermal expansion coefficient and the material dielectric functions, the different forces can be distinguished through their characteristic distance dependencies, their magnitude, and spectral line shape. The ability to unambiguously detect and discriminate optical gradient forces from other photoinduced effects might open exciting prospects for new scanning probe modalities or tip-based opto-nanomechanics. Unlike traditional opto-mechanical resonators, tip−sample junctions can be reliably scaled down to atomic-size cavities, enabling extreme optical confinement and potentially new possibilities to probe and control the dynamics of individual vibrations within molecules or single quantum systems. These may not only have practical implications for photochemistry and photophysics, but also for understanding the coherent control of vibro-polariton states down to the single-photon molecule coupling level. Beyond the thermal effects currently utilized for chemical nanoimaging and spectroscopy, the possibility to optically excite modes that are otherwise difficult to populate might enable the study of thermal nonequilibrium phonon or vibrational populations in the ultrastrong opto-mechanical coupling regime.

■ ASSOCIATED CONTENT

ⓢ Supporting Information

The Supporting Information is available free of charge on the ACS Publications website at DOI: 10.1021/acs.nanolett.8b01899.

> Additional data showing a detail plot of the long-range force shown in Figure 4a), its exponential fit as well as the tapping phase. A plot of the spectrum of the long-range force acquired 15 nm above a 60 nm thick PMMA film, and plots of approach curves acquired using small, down to <3 nm tapping amplitudes. Additional description of the model used to calculate the optical gradient force and its thickness dependence. Topographic image of the tapered PMMA film used for thickness-dependent force measurements (PDF)

■ AUTHOR INFORMATION

Corresponding Author
*E-mail: markus.raschke@colorado.edu.

ORCID Ⓘ
Brian T. O'Callahan: 0000-0001-9835-3207
Eric A. Muller: 0000-0002-9629-1767
Markus B. Raschke: 0000-0003-2822-851X

Notes
The authors declare no competing financial interest.

■ ACKNOWLEDGMENTS

■ REFERENCES

(1) Ashkin, A.; Dziedzic, J. M. *Appl. Phys. Lett.* **1976**, *28*, 333−335.

(2) Bloch, I. *Nat. Phys.* **2005**, *1*, 23−30.

(3) Obrecht, J. M.; Wild, R. J.; Antezza, M.; Pitaevskii, L. P.; Stringari, S.; Cornell, E. A. *Phys. Rev. Lett.* **2007**, *98*, 063201.

(4) Casimir, H. B. G.; Polder, D. *Phys. Rev.* **1948**, *73*, 360−372.

(5) Jahng, J.; Brocious, J.; Fishman, D. A.; Yampolsky, S.; Nowak, D.; Huang, F.; Jahng, J.; Brocious, J.; Fishman, D. A.; Yampolsky, S.; Nowak, D.; Huang, F.; Apkarian, V. A.; Wickramasinghe, H. K. *Appl. Phys. Lett.* **2015**, *106*, 083113.

(6) Huang, F.; Tamma, V. A.; Mardy, Z.; Burdett, J.; Kumar, H. *Sci. Rep.* **2015**, *5*, 10610.

(7) Tumkur, T. U.; Yang, X.; Cerjan, B.; Halas, N. J.; Nordlander, P.; Thomann, I. *Nano Lett.* **2016**, *16*, 7942−7949.

(8) Nowak, D.; Morrison, W.; Wickramasinghe, H. K.; Jahng, J.; Potma, E.; Wan, L.; Ruiz, R.; Albrecht, T. R.; Schmidt, K.; Frommer, J.; Sanders, D. P.; Park, S. *Sci. Adv.* **2016**, *2*, e1501571.

(9) Rajapaksa, I.; Wickramasinghe, H. K. *Appl. Phys. Lett.* **2011**, *99*, 161103.

(10) Rajapaksa, I.; Uenal, K.; Wickramasinghe, H. K.; Rajapaksa, I.; Uenal, K.; Wickramasinghe, H. K. *Appl. Phys. Lett.* **2010**, *97*, 073121.

(11) Lu, F.; Belkin, M. A. *Opt. Express* **2011**, *19*, 19942−19947.

(12) Lahiri, B.; Holland, G.; Centrone, A. *Small* **2013**, *9*, 439−445.

(13) Lu, F.; Jin, M.; Belkin, M. A. *Nat. Photonics* **2014**, *8*, 307−312.

(14) Yang, H. U.; Raschke, M. B. *New J. Phys.* **2016**, *18*, 053042.

(15) Arias-González, J. R.; Nieto-Vesperinas, M.; Lester, M. *Phys. Rev. B: Condens. Matter Mater. Phys.* **2002**, *65*, 115402.

(16) Nieto-Vesperinas, M.; Chaumet, P. C.; Rahmani, A. *Philos. Trans. R. Soc., A* **2004**, *362*, 719−737.

(17) Jahng, J.; Park, S.; Morrison, W. A.; Kwon, H.; Nowak, D.; Potma, E. O.; Lee, E. S. *arXiv:1711.02479v1* 2017, accessed 8/8/2018.

(18) Almajhadi, M.; Wickramasinghe, H. K. *Opt. Express* **2017**, *25*, 26923−26938.

(19) Wang, L. V.; Hu, S. *Science* **2012**, *335*, 1458−1462.

(20) Knoll, B.; Keilmann, F. *Opt. Commun.* **2000**, *182*, 321−328.

(21) Jahng, J.; Kim, B.; Lee, E. S.; Potma, E. O. *Phys. Rev. B: Condens. Matter Mater. Phys.* **2016**, *94*, 195407.

(22) Pollard, B.; Muller, E. A.; Hinrichs, K.; Raschke, M. B. *Nat. Commun.* **2014**, *5*, 3587.

(23) Ladani, F. T.; Potma, E. O. *Phys. Rev. B: Condens. Matter Mater. Phys.* **2017**, *95*, 205440.

(24) Taubner, T.; Keilmann, F.; Hillenbrand, R. *Nano Lett.* **2004**, *4*, 1669−1672.

(25) Jones, A. C.; Raschke, M. B. *Nano Lett.* **2012**, *12*, 1475−1481.

(26) Atkin, J. M.; Sass, P. M.; Teichen, P. E.; Eaves, J. D.; Raschke, M. B. *J. Phys. Chem. Lett.* **2015**, *6*, 4616−4621.

(27) James, P. J.; Antognozzi, M.; Tamayo, J.; McMaster, T. J.; Newton, J. M.; Miles, M. J. *Langmuir* **2001**, *17*, 349−360.

(28) Hu, S.; Raman, A. *Nanotechnology* **2008**, *19*, 375704.

(29) García, R.; Pérez, R. *Surf. Sci. Rep.* **2002**, *47*, 197−301.

(30) Cvitkovic, A.; Ocelic, N.; Hillenbrand, R. *Opt. Express* **2007**, *15*, 8550−8565.

(31) Chae, J.; An, S.; Ramer, G.; Stavila, V.; Holland, G.; Yoon, Y.; Talin, A. A.; Allendorf, M.; Aksyuk, V. A.; Centrone, A. *Nano Lett.* **2017**, *17*, 5587−5594.

(32) Jahng, J.; Brocious, J.; Fishman, D. A.; Huang, F.; Li, X.; Tamma, V. A.; Wickramasinghe, H. K.; Potma, E. O. *Phys. Rev. B: Condens. Matter Mater. Phys.* **2014**, *90*, 155417.

(33) Sasihithlu, K.; Pendry, J.; Craster, R. *Z. Naturforsch., A: Phys. Sci.* **2017**, *72*, 181−188.

(34) Pendry, J. B.; Sasihithlu, K.; Craster, R. V. *Phys. Rev. B: Condens. Matter Mater. Phys.* **2016**, *94*, 075414.

(35) Günther, P.; Fischer, U. C.; Dransfeld, K. *Appl. Phys. B: Photophys. Laser Chem.* **1989**, *48*, 89−92.

(36) Degertekin, F. L.; Hadimioglu, B.; Sulchek, T.; Quate, C. F. *Appl. Phys. Lett.* **2001**, *78*, 1628−1630.

(37) Katzenmeyer, A. M.; Holland, G.; Kjoller, K.; Centrone, A. *Anal. Chem.* **2015**, *87*, 3154−3159.